Time series of bio-optical properties in a subtropical gyre: Implications for the evaluation of interannual trends of biogeochemical properties

ZhongPing Lee,[1] Shaoling Shang,[2] Chuanmin Hu,[3] Marlon Lewis,[4] Robert Arnone,[5] Yonghong Li,[2] and Bertrand Lubac[5]

Received 29 September 2009; revised 12 April 2010; accepted 25 May 2010; published 14 September 2010.

[1] With a validated Quasi-Analytical Algorithm, an 11 year (1998–2008) monthly time series of the primary optical properties of waters in the center of the South Pacific gyre was developed from Sea-viewing Wide Field-of-view Sensor (SeaWiFS) and Moderate Resolution Imaging Spectroradiometer (MODIS). Also derived are chlorophyll *a* (Chl *a*) concentrations with the operational empirical algorithms for SeaWiFS and MODIS. The optical properties include the absorption coefficient (at 443 nm) of phytoplankton (a_{ph}) and that of the combination of detritus and gelbstoff (a_{dg}). From these time series, we further derived their annual background (summer low) and seasonal intensity (the difference between winter high and summer low). These time series show that (1) the optical properties have different seasonal and interannual variations, indicating different dynamics of these properties in the subtropical gyre; (2) there is a decreasing trend ($r^2 = 0.24$) of the background a_{ph} in the 1998–2008 period and an increasing trend of the a_{ph} seasonal intensity ($r^2 = 0.11$) for this period, and both trends are not statistically significant; (3) the a_{ph} time series agrees with the Chl *a* time series at the seasonal scale, but differs with respect to interannual variations; and (4) different interannual trends could be inferred with different time frames. These results emphasize that it is difficult to draw unequivocal conclusions about long-term trends of biogeochemical properties in the oceans with the current relatively short bio-optical records. To clarify and predict such trends, it is critical to get a full account of the forces that are responsible for the seasonal and interannual variations of these properties.

Citation: Lee, Z. P., S. Shang, C. Hu, M. Lewis, R. Arnone, Y. Li, and B. Lubac (2010), Time series of bio-optical properties in a subtropical gyre: Implications for the evaluation of interannual trends of biogeochemical properties, *J. Geophys. Res.*, *115*, C09012, doi:10.1029/2009JC005865.

1. Introduction

[2] Subtropical gyres are not only important for studies of ocean biogeochemistry and the global carbon cycle [*Behrenfeld et al.*, 2006; *McClain et al.*, 2004], they are also important for the detection of anthropogenic climate change [*Barnett et al.*, 2001]. Recent studies based on chlorophyll *a* (Chl *a*) concentration, derived from satellite ocean color measurements, have shown that Chl *a* in the subtropical gyres is showing a waning trend [*Gregg et al.*, 2005] and that the areas of low Chl *a* gyres are expanding [*McClain et al.*, 2004; *Polovina et al.*, 2008]. These results [*Gregg et al.*, 2005; *Polovina et al.*, 2008] imply a reduced production of phytoplankton in surface waters of the gyres in the past decade and contribute to speculation that such an annual declining trend could be a result of enhanced surface water stratification due to temperature increases [*Gregg et al.*, 2005; *Polovina et al.*, 2008]. However, each of these studies used a single time window to estimate long-term trends with the consequent possibility of alias. Further, when analyzing satellite observations, these studies used Chl *a* that was derived with an empirical algorithm developed and validated with global data sets [*O'Reilly et al.*, 1998] and not specifically validated for waters in the gyres. Such empirical algorithms use the blue-green ratio of ocean color to derive Chl *a*, where the potentially confounding impacts of gelbstoff (or colored dissolved organic matter (CDOM)) could not be removed [*Carder et al.*, 1991].

[3] Here, we use in situ bio-optical data measured near the surface center of the South Pacific gyre to show that absorption coefficients of gelbstoff and phytoplankton of such extremely clear waters can be derived with high accuracy from remote sensing reflectance with a semianalytical

[1]Geosystems Research Institute, Mississippi State University, John C. Stennis Space Center, Mississippi, USA.
[2]State Key Laboratory of Marine Environmental Science, Xiamen University, Xiamen, China.
[3]College of Marine Science, University of South Florida, St. Petersburg, Florida, USA.
[4]Department of Oceanography, Dalhousie University, Halifax, Nova Scotia, Canada.
[5]Naval Research Laboratory, John C. Stennis Space Center, Mississippi, USA.

0148-0227/10/2009JC005865

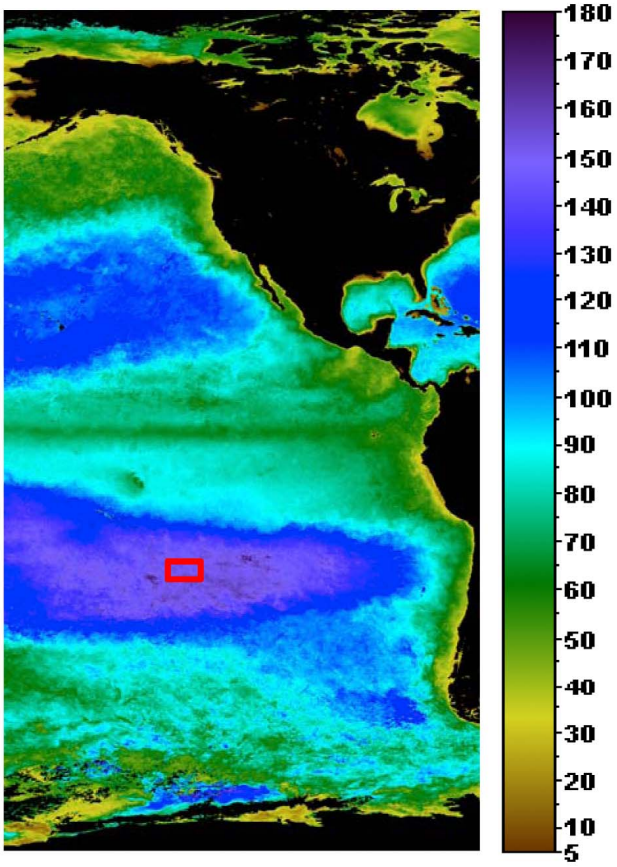

Figure 1. Location of the study site (23–28°S, 130–140°W). The background image is the annual water clarity (measured by euphotic depth in meters; see the work of *Lee et al.* [2007] algorithm) for 2008 (from Ocean Biology Processing Group).

algorithm. We then use this algorithm to develop an 11 year (January 1998–December 2008) monthly time series of absorption coefficients for phytoplankton and gelbstoff based on ocean color radiometric data from the Sea-viewing Wide Field-of-view Sensor (SeaWiFS) and the Moderate Resolution Imaging Spectrometer (MODIS) (both operated by NASA [*McClain*, 2009]). A monthly time series of Chl *a* was also derived from the same SeaWiFS and MODIS data with the operational empirical algorithms (OC4v4 and OC3m) [*O'Reilly et al.*, 2000]. Seasonal and interannual variations were evaluated, and interannual trends were analyzed with different time frames. Results from these studies indicate that (1) a long-term (decades) record of ocean color observations is required to deduce unequivocal trends of biogeochemical properties in the oceans and (2) it is more important to account for the forces that are responsible for the seasonal and interannual variations, as such forces are the foundation to understand and eventually predict the apparent trends, if any.

2. Data and Method

2.1. In Situ Data for Algorithm Validation

[4] Remote sensing spectral reflectance ($R_{rs}(\lambda)$; sr^{-1}; ratio of water-leaving radiance to downwelling irradiance above sea surface) for five stations (STB4, STB5, STB8, GYR4, and GYR5 that are listed in Table 1 of *Morel et al.* [2007]) in the South Pacific gyre was computed from direct measurements of downwelling irradiance above the sea surface ($E_s(\lambda)$; W $m^{-2}nm^{-1}$) and nadir upwelling radiance ($L_u(\lambda)$; W $m^{-2}nm^{-1}sr^{-1}$). Measurement of $E_s(\lambda)$ was taken aboard ship while measurement of $L_u(\lambda)$ was made at a depth of 20 cm below the ocean surface using a modified hyperspectral profiling radiometer (HyperoPro, Satlantic, Inc.) adapted to float at the sea surface and tethered such that the instrument operated at a distance of ~100 m from the vessel. Instrument tilt was measured directly, and measurements were rejected if tilts exceeded 5°. Measurements were made over the wave band 380–800 nm with a spectral resolution of 3.3 nm, with each band having a half-maximum band pass of 10 nm. Dark values were taken every five samples by use of an internal shutter. These were linearly interpolated for each light value, and then subtracted from the observations. Calibration coefficients and corrections for immersion effects were obtained following standard protocols [*Mueller et al.*, 2003] and applied to the measurements; demonstrated absolute accuracies are <2.8% for radiance and <2.1% for irradiance [*Gordon et al.*, 2009]. Irradiance and radiance data were taken for 3 min at each deployment, with each observation within the deployment time series representing integration times of 0.03 to 0.5 s, depending on the intensity of the incident (ir)radiance. These measurements were then interpolated to a common time frame at a frequency of every 2 s and to a common spectral resolution of every 2 nm.

[5] Upwelling radiance measurements were then propagated to the sea surface using an iterative approach [*Mueller et al.*, 2003] that estimates the spectral diffuse attenuation coefficient from spectral ratios of measured radiance, and the nadir water-leaving radiance above the sea surface, $L_W(\lambda)$, is then computed based on Fresnel reflectance and the real relative index of refraction [*Mueller et al.*, 2003]. A 3 min time series of R_{rs} was made by dividing the computed water-leaving radiance by the downward irradiance for each time interval, and an average value and standard deviation was computed for each deployment.

[6] Concurrent data of inherent optical properties (IOP: the total absorption coefficient (a; m^{-1}) and the portion attributable to particulates (a_p; m^{-1}) at 420 nm) of these stations were measured and presented in Table 1 in the work of *Morel et al.* [2007]. The absorption coefficient attributable to yellow substance or gelbstoff (a_g; m^{-1}) at 420 nm is estimated from the presented $a_g(310)$ value, with a spectral slope equal to 0.0203 nm^{-1} (for the wavelength range of 300–500 nm) reported in the same article. No particle backscattering coefficients (b_{bp}) are listed, but they can be inferred from the work of *Huot et al.* [2008] and *Twardowski et al.* [2007] that $b_{bp}(550)$ was in a range of 0.0002–0.0004 m^{-1} based on the listed Chl *a* values.

2.2. Satellite Data for Temporal Studies

[7] The research site selected to study the temporal variations of optical and biological (Chl *a*) properties is a small box (23–28°S, 130–140°W) in the South Pacific gyre (see Figure 1), which approximates the surface center of this gyre where the spatial distribution of bio-optical properties are nearly uniform [*Behrenfeld et al.*, 2005; *McClain et al.*, 2004]. This site was also selected because (1) the waters are

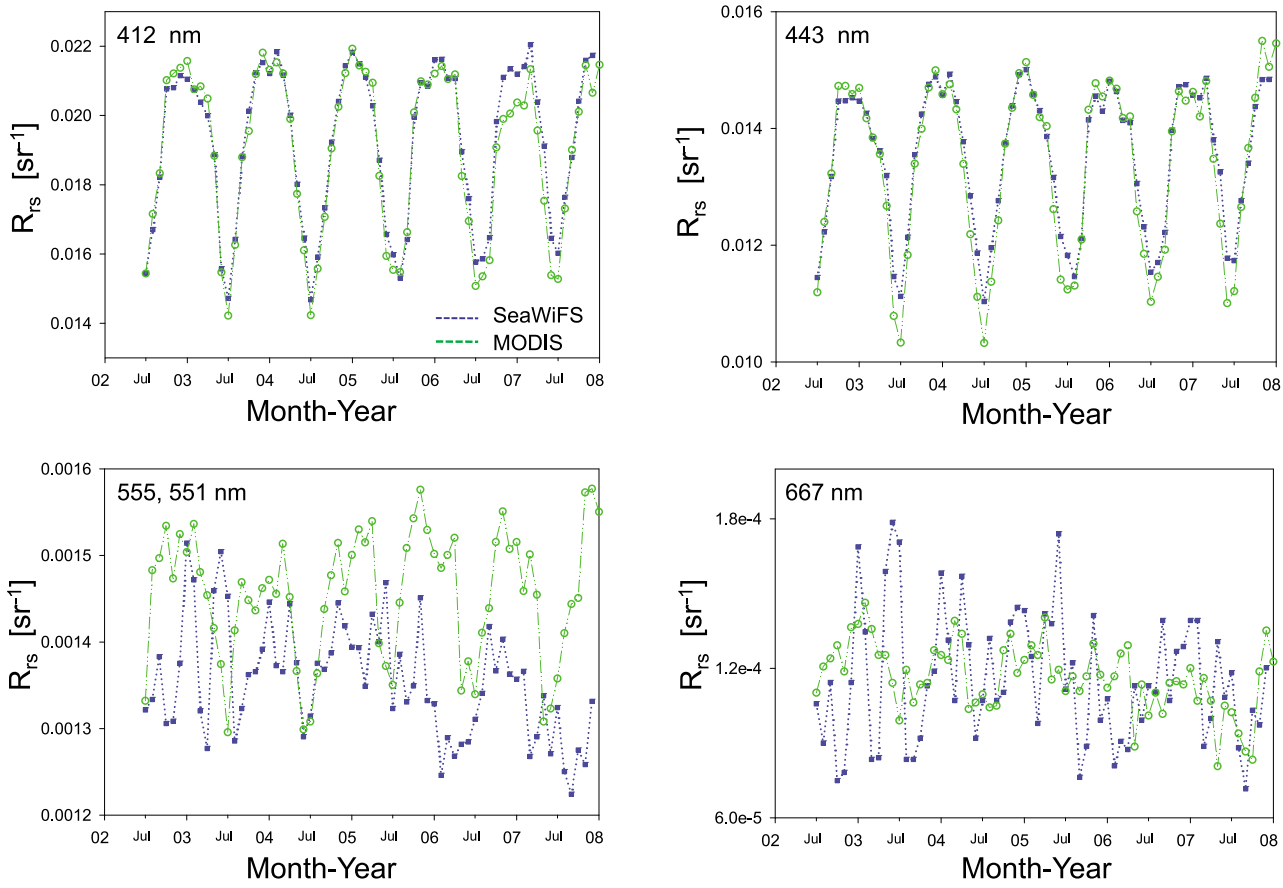

Figure 2. Comparison of remote sensing reflectance between SeaWiFS (solid squares) and MODIS (open circles) measurements.

the "clearest" of the world's oceans [*Morel et al.*, 2007], thus it is easier to detect changes of biogeochemical properties, if any, and (2) the spatial gradient is minimum [*Behrenfeld et al.*, 2005], thus changes observed here approximate local changes instead of results of advection. In addition, there are recent bio-optical measurements measured in this gyre (see section 2.1) to validate algorithms for remote sensing retrievals.

[8] For all pixels in this box, monthly binned normalized water-leaving spectral radiance ($L_{WN}(\lambda)$) data with a 9 km resolution were downloaded from the OceanColor Web portal (http://oceancolor.gsfc.nasa.gov) that is operated by the Ocean Biology Processing Group supported by NASA. These $L_{WN}(\lambda)$ values include those from SeaWiFS (412, 443, 490, 510, 555, and 667 nm; January 1998 to December 2007; after reprocessing 5.2) and those from MODIS-Aqua (412, 443, 488, 531, 551, and 667 nm; from July 2002 to December 2008; after reprocessing 1.1). In order to minimize impacts of random spikes on the inverted products and analysis that followed, for each month (and each sensor) the top and bottom 10% of the values within the box were excluded before a spatially averaged $L_{WN}(\lambda)$ was calculated. We also compared the median value with the average for each band and found that the two were nearly identical (the differences were under 0.5%). Therefore, this average value was used to represent the property of the study site for that sensor. The multiband $L_{WN}(\lambda)$ values were then converted to multiband remote sensing reflectance ($R_{rs}(\lambda)$) by dividing $L_{WN}(\lambda)$ by the extraterrestrial solar spectral irradiance ($F_0(\lambda)$) [*Gordon*, 2005].

[9] The remote sensing reflectance values at 667 nm from SeaWiFS ($R_{rs}(667)$) were around 0.00026 sr^{-1}, which are considerably higher than that from MODIS (~0.00012 sr^{-1}) for such clear waters [*Franz*, 2009]. As $R_{rs}(667)$ is generally between 0.00005 and 0.00016 sr^{-1} for particulate backscatter values, $b_{bp}(667)$, between 0 and 0.001 m^{-1} based on Hydrolight [*Mobley*, 1995] simulations, these high values suggest a bias (overestimation) of SeaWiFS $R_{rs}(\lambda)$ [also see *Franz*, 2009] for these waters (note that $b_{bp}(532)$ here is ~0.0002 m^{-1} [*Twardowski et al.*, 2007]). To be more consistent with theoretical predictions and those from MODIS, we adjusted the SeaWiFS $R_{rs}(\lambda)$ by subtracting an offset of 0.000175 sr^{-1} for all bands (0.000175 sr^{-1} was deduced by forcing the average of SeaWiFS $R_{rs}(667)$ to be equal to the average of MODIS $R_{rs}(667)$).

[10] Figure 2 presents the time series of adjusted SeaWiFS R_{rs} at 412, 443, 55x (555 for SeaWiFS, 551 for MODIS), and 667 nm along with those from MODIS for the 2002–2007 period. Clearly, the two sets of R_{rs} match each other very well (~2.2% average percentage difference) at the 412 and 443 nm bands (the two spectral channels that are critical for analytically separating contributions of gelbstoff and phytoplankton), although slightly larger (~5%) differences do exist at 412 nm in the Austral summer of 2007. The consistency of R_{rs} provides us a confidence to achieve longer time series by

combining and merging SeaWiFS and MODIS observations. SeaWiFS $R_{rs}(555)$ is slightly (~7.6%) lower than that of MODIS $R_{rs}(551)$ because of the slightly different band centers, and its seasonal pattern is subdued. Compared to MODIS $R_{rs}(667)$, SeaWiFS $R_{rs}(667)$ is quite noisy with no apparent seasonal patterns. These reduced seasonal features in R_{rs} are due to the smaller digitization (10 bit) of the SeaWiFS sensor [*Hu et al.*, 2001].

[11] For analysis and comparison, we downloaded the sea surface temperature (SST) products released by the Physical Oceanography Distributed Active Archive Center at the NASA Jet Propulsion Laboratory (Pasadena, CA, http://podaac.jpl.nasa.gov), which was measured by NOAA AVHRR Pathfinder and has a spatial resolution of 9 × 9 km. A spatially averaged SST, similar to the processing of L_{WN} data, was obtained to represent the monthly time series from 1998 to 2008.

2.3. Inversion Method

2.3.1. Correction of Raman Scattering

[12] Water-leaving radiance is composed of contributions from elastic and inelastic scatterings [*Lee et al.*, 1994; *Mobley*, 1994; *Sathyendranath and Platt*, 1997]. The latter part includes Raman scattering [*Stavn and Weidemann*, 1988], and fluorescence from chlorophyll [*Gordon*, 1979; *Yentsch and Phinney*, 1985] and gelbstoff [*Lee et al.*, 1994; S. K. Hawes et al., Quantum fluorescence efficiencies of marine humic and fulvic acids: Effects on ocean color and fluorometric detection, paper presented at Ocean Optics, 1992]. In this study, we ignored fluorescence because both were very weak (<1% to R_{rs}) for such extremely clear waters. On the other hand, since water constituents are scarce in the gyres [*Morel et al.*, 2007], there is sufficient blue-green sunlight in the water column to stimulate Raman scattering, whose contribution to R_{rs} is then not negligible [*Hu and Voss*, 1997; *Marshall and Smith*, 1990; *Sathyendranath and Platt*, 1998; *Stavn and Weidemann*, 1988]. This effect needs to be accounted for when an analytical inversion algorithm is applied. Unlike the R_{rs} models for elastic scattering (which are generally functions of IOPs) [*Gordon et al.*, 1988; *Sathyendranath and Platt*, 1997], Raman contribution to R_{rs} is not only a function of IOPs, but also a function of incident irradiance at the input and output wavelengths [*Lee et al.*, 1994; *Marshall and Smith*, 1990]. For R_{rs} from SeaWiFS and MODIS measurements, however, no such data are available. To overcome the shortage of such data, an empirical approach (based on radiative transfer simulations) was applied to correct contributions from Raman scattering, similar to the work of *Loisel and Stramski* [2000].

[13] Using Hydrolight [*Mobley*, 1995], simulations with and without Raman scattering were carried out for chlorophyll a concentrations equal to 0.01 and 0.03 mg/m^3 ($a(440)$ between 0.008 and 0.013 m^{-1}), and for solar zenith angles equal to 10° and 70°, respectively. From these simulations, the ratio of R_{rs} without Raman scattering ($R_{rs,no\text{-}Raman}$) to R_{rs} with Raman scattering ($R_{rs,with\text{-}Raman}$) was calculated ($rr = R_{rs,no\text{-}Raman}/R_{rs,with\text{-}Raman}$). These rr were around 0.96, 0.95, 0.89, 0.85, and 0.84 for 410, 440, 490, 550, and 670 nm, respectively, and were quite stable (within 5%) for these simulations. On the basis of these analyses, a correction of Raman scattering to SeaWiFS/MODIS measured R_{rs} was taken as rr times satellite R_{rs}, and this product was then used with the analytical algorithm for further data processing. Without such a correction, the derived b_{bp} (via analytical algorithms) could be elevated by as much as 60% for such clear waters.

2.3.2. Inversion of IOPs

[14] Previous studies [*Gregg et al.*, 2005; *McClain et al.*, 2004; *Palter et al.*, 2005; *Polovina et al.*, 2008] regarding the oceanic gyres were based on the empirically derived chlorophyll a concentration from the observation of ocean color [*O'Reilly et al.*, 2000]. However, such empirical algorithms do not separate the optical contributions of gelbstoff from that of phytoplankton pigments. Consequently, gelbstoff signals may be "seen" as phytoplankton [*Carder et al.*, 1989]. To delineate the phytoplankton property with higher fidelity, we used a semianalytical algorithm [*Lee et al.*, 2002, 2007] to derive the absorption coefficient (at 443 nm) of phytoplankton (a_{ph}) and that of the combination of detritus and gelbstoff (a_{dg}), respectively, as well as the particle backscattering coefficient (b_{bp}). Note that this b_{bp} is a collective index representing all other scattering contributors [*Stramski et al.*, 2001, 2004] aside from water molecules (or "pure" seawater).

[15] Because molecular scattering makes the primary contribution to remote sensing reflectance in the blue-green wavelengths, the effects of the molecular scattering phase function need to be well accounted for [*Lee et al.*, 1994, 2004; *Morel and Gentili*, 1991; *Sathyendranath and Platt*, 1997]. We therefore used a modified analytical function for R_{rs} [*Lee et al.*, 2009] based on the model of *Lee et al.* [2004] that explicitly separates the phase-function effects of molecular and particle scattering:

$$R_{rs}(\lambda,\Omega) = \left(G_0^w(\Omega) + G_1^w(\Omega)\frac{b_{bw}(\lambda)}{\kappa(\lambda)}\right)\frac{b_{bw}(\lambda)}{\kappa(\lambda)} + \left(G_0^p(\Omega) + G_1^p(\Omega)\frac{b_{bp}(\lambda)}{\kappa(\lambda)}\right)\frac{b_{bp}(\lambda)}{\kappa(\lambda)}, \quad (1)$$

with $\kappa = a + b_b$, and $b_b = b_{bw} + b_{bp}$. Here Ω represents generally the Sun-sensor angular geometry for the remote sensing reflectance and taken as that of normalized water-leaving radiance in this study. a and b_b are the total absorption and backscattering coefficients, respectively, while b_{bw} is the backscattering coefficient of pure seawater (all m^{-1}). Values of the model parameters ($G_0^w(\Omega)$, $G_1^w(\Omega)$, $G_0^p(\Omega)$, and $G_1^p(\Omega)$; sr^{-1}) for various Sun angles and viewing geometries have been developed based on Hydrolight simulations [*Lee et al.*, 2009]. For normalized water-leaving radiance [*Gordon*, 2005], the G parameters are 0.0604, 0.0406, 0.0402, and 0.1310 sr^{-1} when particle scattering takes a blended phase function [*International Ocean-Colour Coordinating Group* (*IOCCG*), 2006].

[16] In the inversion process, the backscattering and absorption coefficients of pure seawater are based on the work of *Zhang et al.* [2009] and *Pope and Fry* [1997], respectively. $b_{bw}(\lambda)$ is calculated with a salinity value of 38.4‰ [*Zhang et al.*, 2009]. When the total absorption coefficient was decomposed into the contributions of phytoplankton and detritus/gelbstoff [*Lee et al.*, 2002], the ratio of $a_{ph}(412)/a_{ph}(443) = 0.742$ was used for such low chlorophyll waters [*Bricaud et al.*, 2010], and the ratio of $a_{dg}(412)/a_{dg}(443) = 1.592$ was used, which was calculated with a spectral slope of 0.015 nm^{-1} [*Morel et al.*, 2007; *Twardowski*

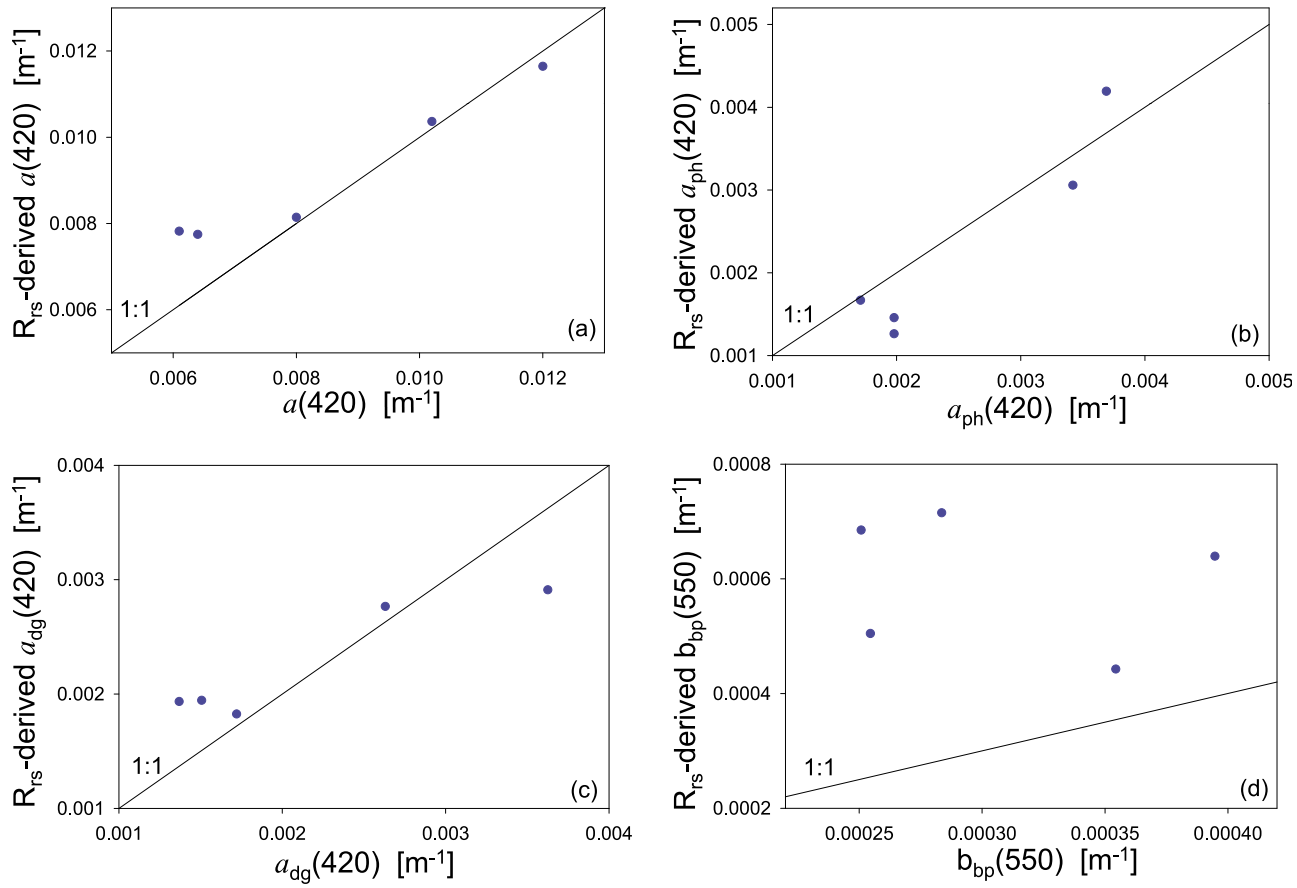

Figure 3. For measurements made in the South Pacific gyre (November 2004), remote sensing inversions are compared with values determined independently by other means. (a) Total absorption, (b) phytoplankton pigment absorption, (c) detritus/gelbstoff absorption, and (d) particle backscattering coefficient at 550 nm (values representing *x* axis were estimate based upon chlorophyll *a* concentration, see section 3.1). Values for *x* axis were based on Table 1 in the work of *Morel et al.* [2007].

et al., 2004; *Bricaud et al.*, 2010] when spectral a_{dg} is modeled as an exponential decay function of wavelength [*Bricaud et al.*, 1981]. This spectral slope, which differs from that reported by *Morel et al.* [2007] because of differences in wavelength ranges, is based on measurements in NOMAD [*Werdell and Bailey*, 2005] (also see http://www.ioccg.org/groups/Software_OCA/QAA_v5.pdf).

3. Results and Discussion

3.1. In Situ Data

[17] We used data published by *Morel et al.* [2007] to evaluate the inversion performance. Figure 3 compares R_{rs}-derived a(420), a_{ph}(420), and a_{dg}(420) with those presented in Table 1 in the work of *Morel et al.* [2007]. a_{ph}(420) and a_{dg}(420) that represent sample measurements were converted from the measured a_p(420) and a_g(420) [*Morel et al.*, 2007], with a_d(420) considered 10% of a_p(420) (a_{ph}(420) then equals a_p(420) − a_d(420)), and this a_d(420) was added to a_g(420) to make a_{dg}(420)). The 10% value was estimated based on previous reports [*Siegel et al.*, 2002; *Morel et al.*, 2007] that detritus absorption makes a small portion of particulate absorption for such extremely clear waters.

[18] As described in detail by *Morel et al.* [2007], the optical values are extremely low for this oligotrophic water in November (only a couple of months after the winter bloom [*McClain et al.*, 2004]), with a(420) in a range of 0.006–0.012 m^{-1}, a_{ph}(420) between 0.0017 and 0.0037 m^{-1}, and a_{dg}(420) between 0.0014 and 0.0036 m^{-1}. These extremely low values, all from sample measurements, are the fundamental reasons why the water appears "violet blue" [*Morel et al.*, 2007]. The root-mean-square differences in linear scale between R_{rs}-derived and published absorption coefficients are ~0.0010 m^{-1}, 0.0005 m^{-1}, and 0.0005 m^{-1} for a(420), a_{ph}(420), and a_{dg}(420), respectively. These differences are equivalent or smaller than the measurement precision for existing instruments/methods for oceanic measurements [*Twardowski et al.*, 2007]. On a relative scale, the averaged percentage differences (average of |measured − R_{rs}-derived|/measured) for the three optical properties are ~11%, ~18%, and ~20%, respectively. If a_d(420) is considered as 5% of a_p(420), the average percentage differences for a_{ph}(420) and a_{dg}(420) become ~20% and ~26%, respectively. Considering that values for both the *x* and *y* axes are associated with uncertainties [*Lee et al.*, 2010], these comparisons confirm that inherent optical properties derived from measured R_{rs} are as good as those determined by direct

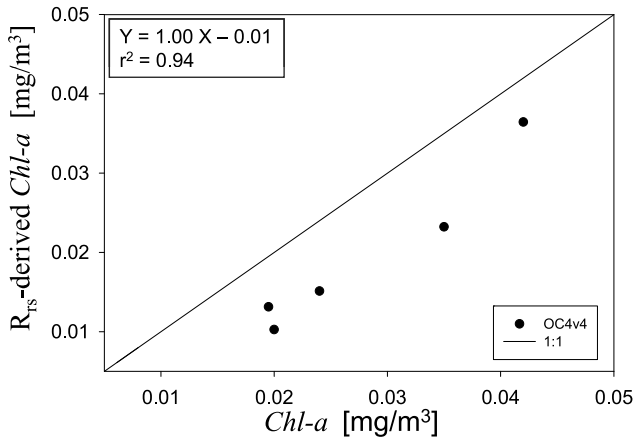

Figure 4. Same as Figure 3, but for comparison of Chl *a*. The OC4v4 algorithm was used for the derivation of Chl *a* from reflectance.

measurement [*Morel et al.*, 2007], at least to the measurements made in November 2004. Inversion algorithms can therefore derive highly reliable absorption coefficients from R_{rs} for such extremely clear waters, as has been recently shown true for other oligotrophic and mesotrophic environments [*Gordon et al.*, 2009]. This robust conclusion is particularly important for applying such algorithms to satellite data to obtain long-term observations of these optical properties of such waters, although additional uncertainty from satellite measurements will be introduced [*Antoine et al.*, 2008]. For waters in the open ocean, especially gyres, less uncertainty (<10%) in satellite-measured R_{rs} is expected because of the stronger water-leaving radiances in the blue-green wavelengths and the easier handling of atmosphere corrections [*Antoine et al.*, 2008; *Gordon and Wang*, 1994].

[19] The R_{rs}-derived particle backscattering coefficient at 550 nm ($b_{bp}(550)$) is approximately 0.0006 m^{-1} for the five stations (see Figure 3d). This is higher (by ~0.0003 m^{-1}) than the particle backscattering coefficient inferred from the measured chlorophyll *a* concentrations [*Huot et al.*, 2008; *Twardowski et al.*, 2007]. In addition, the two sets of b_{bp} are not correlated. Reasons for these differences, although they are in fact within the measurement precision [*Twardowski et al.*, 2007], include uncertainties in both in situ measurement and remote sensing retrievals as well as other factors that are not yet included in the inversion process. Such factors include effects of particle phase function shape [*Mobley et al.*, 2002], scattering from bubbles [*Zhang et al.*, 1998], and wave-focusing effects [*Zaneveld et al.*, 2001]. Methods to correct these secondary effects are still under development.

[20] For the same data set, when Chl *a* derived from R_{rs} with the OC4v4 algorithm [*O'Reilly et al.*, 2000] is compared with Chl *a* from water samples (Figure 4), the average percentage difference is ~37%, which is a greater relative discrepancy than that of $a_{ph}(420)$ and $a_{dg}(420)$ (much higher than that of $a(420)$). It appears that most of the difference came from a systematic bias (underestimation by ~0.01 mg/m^3) of remotely sensed Chl *a* (coefficient of determination r^2 = 0.94). This may not be surprise as the coefficients employed by the OC4v4 (or OC3m) algorithm were derived empirically so that a "best fit" was achieved for a "global" data set that covers various regions at various temporal cycles [*O'Reilly et al.*, 1998].

3.2. Satellite Data

3.2.1. Time Series of Bio-optical Properties

[21] With the above validated semianalytical algorithm, monthly $a(443)$, $a_{ph}(443)$, and $a_{dg}(443)$ of the study site were derived from the monthly R_{rs} time series measured by SeaWiFS and MODIS, respectively. The particulate backscattering coefficient, $b_{bp}(551)$, was also derived from both measurements, and they are generally in a range of 0.0004–0.0007 m^{-1}. However, because of the relatively large uncertainty between retrieved and measured b_{bp} (Figure 3d), we omitted the evaluation of b_{bp} temporal variations in this study, although generally an inverse correlation was found between R_{rs}-derived a_{ph} and R_{rs}-derived b_{bp}. Figure 5 presents the inverted absorption properties between January 1998 and December 2008, with thick symbols indicating values between July 2002 and December 2007, a period with overlapping measurements from both SeaWiFS and MODIS. For the three absorption properties (a, a_{ph}, and a_{dg}; wavelength dependency is suppressed for clarity) derived from both SeaWiFS and MODIS, the coefficients of determination (r^2) between SeaWiFS and MODIS inversions are 0.93, 0.75, and 0.84, respectively, and the average percentage differences are 3.6%, 12.5%, and 16.4%. These differences are significantly smaller than the seasonal variations of these properties (a: ~45%, a_{ph}: ~80%, and a_{dg}: ~300%). The slightly larger percentage difference for a_{dg} results partially from the extremely low values in the denominator and a larger discrepancy of $R_{rs}(412)$ in the Austral summer of 2007 (see Figure 2).

[22] For the Chl *a* values derived empirically from SeaWiFS and MODIS (Figure 5d), the average percentage difference is 15.2% (r^2 = 0.81) for the July 2002–December 2007 period. The larger percentage difference and smaller r^2 value (compared to the results of $a(443)$) suggest a slight discrepancy introduced by the two empirical algorithms adopted for each sensor. Nevertheless, as the differences from sensors and algorithms are much smaller than the seasonal variations, these results indicate that the bio-optical properties obtained from the two sensors are not only consistent in their temporal patterns, but also in agreement in their absolute magnitudes.

[23] Because of this consistency, the following analyses and discussions regarding the temporal changes of these bio-optical properties are primarily based on a merged time series from SeaWiFS and MODIS retrievals. On the other hand, because SeaWiFS measurements covered 1998 to 2007, discussions based solely on SeaWiFS measurements are also provided. The data merging approach is similar to that of *Maritorena and Siegel* [2005] [also see *IOCCG*, 2007], and the 11 year merged monthly time series is:

$$\begin{cases} P = P(\text{SeaWiFS}), \text{ in and before June 2002;} \\ P = (P(\text{SeaWiFS}) + P(\text{MODIS}))/2, \text{ between July 2002} \\ \quad \text{and December 2007;} \\ P = P(\text{MODIS}), \text{ in and after January 2008.} \end{cases} \quad (2)$$

where P represents a_{ph}, a_{dg}, and Chl *a*.

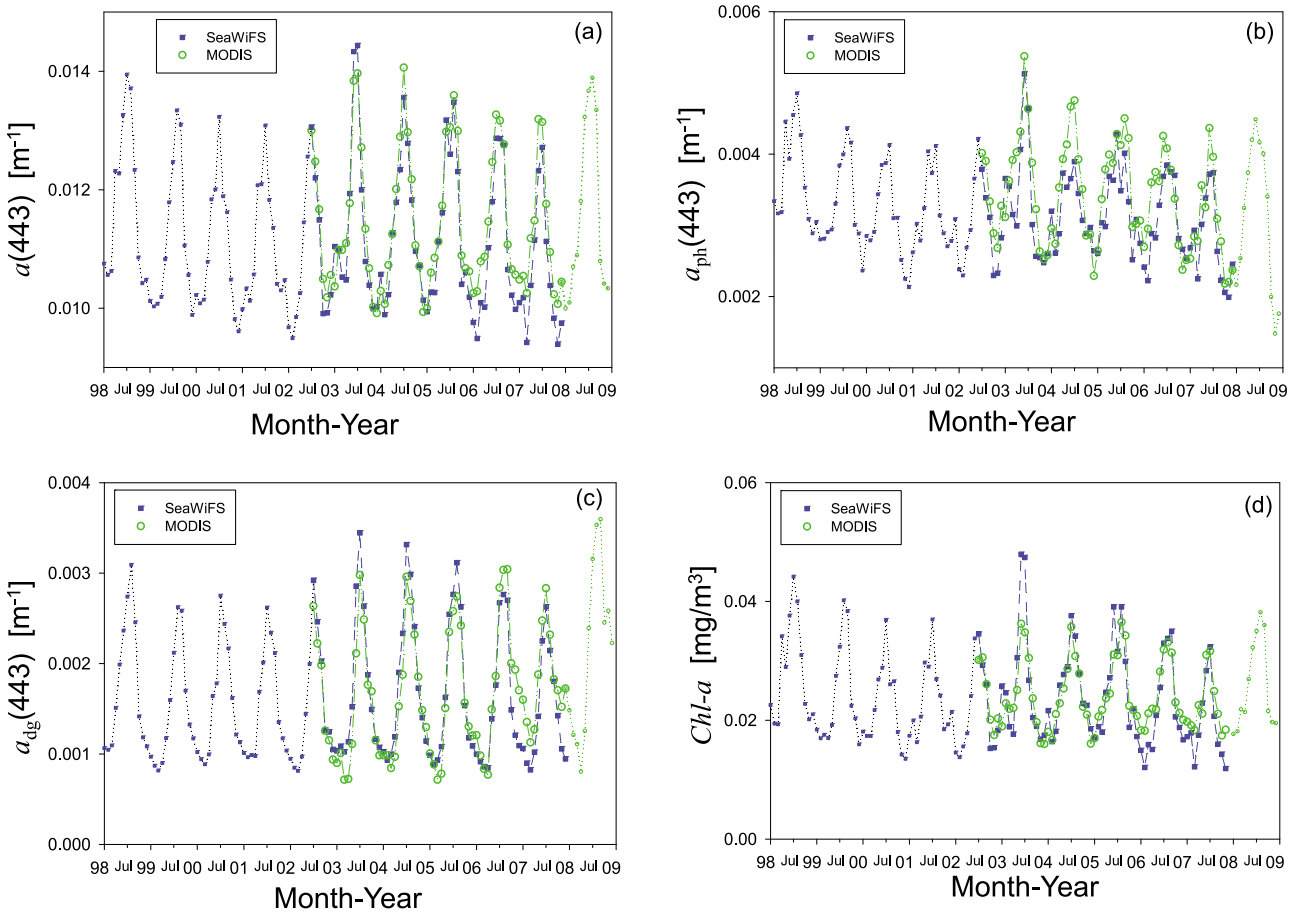

Figure 5. Comparison of inverted bio-optical properties from SeaWiFS (solid squares) and MODIS (open circles) R_{rs}.

3.2.2. Seasonal Variations

[24] To demonstrate the seasonal dynamics of these bio-optical properties, merged monthly properties and the monthly time series of SST are presented in Figures 6a–6c. Clearly, all optical properties and SST show well-pronounced seasonality, but each has its own timing with respect to seasonal highs and lows, as highlighted in Figures 6c and 6d.

[25] The phytoplankton absorption, $a_{ph}(443)$, peaks (~0.0045 m^{-1}) in the months of June–July (Austral winter) and troughs (~0.0025 m^{-1}) in the months of December–January (Austral summer), consistent with the temporal patterns of the empirically derived Chl *a* (Figure 5d) and those from earlier studies [*McClain et al.*, 2004; *Winn et al.*, 1995]. However, the a_{ph} peaks do not coincide with the SST troughs (August–September), but rather occur before SST reaches the winter minima (Figure 6a). This relationship agrees with general phytoplankton dynamics where increases in biomass are associated with enhanced vertical mixing, which delivers the deepwater nutrients [*McClain et al.*, 2004], as June through August is a transition period with SST in a strong decline. This may explain a low coefficient of determination ($r^2 = 0.09$) between a_{ph} and SST during the 1998–2008 period (a comparable result is found between SeaWiFS a_{ph} and SST for the 1998–2007 period). Also note that the a_{ph} troughs follow the SST minima by approximately 2 months [*McClain et al.*, 2004], suggesting a combined effect of nutrient depletion and reduced solar radiation on phytoplankton photosynthesis. More detailed descriptions on seasonal variations of phytoplankton in subtropical gyres can be found in the work of *McClain et al.* [2004].

[26] Different from the relatively mild seasonal variation of a_{ph}, a_{dg} shows much stronger seasonality (~0.0008 m^{-1} in summer to ~0.003 m^{-1} in winter, Figure 6b) at this location. Such strong seasonal variations of a_{dg} will in turn impact the phytoplankton dynamics as a_{dg} directly modulates UV radiation in the upper water column [*Cullen and Neale*, 1994; *Tedetti et al.*, 2007]. Separately, a_{dg} not only shows sharp increases and decreases around the Austral winter, the seasonal highs and lows of a_{dg} do not coincide with that of a_{ph} (Figure 6c), consistent with the observation of a phase delay found in North Atlantic waters [*Hu et al.*, 2006]. The independent a_{dg} seasonality can be further manifested with the a_{dg}/a_{ph} ratio [*Hu et al.*, 2006; *Jolliff et al.*, 2008], where a wide range of seasonal variation (~0.3–0.8) is found for this location (see Figure 6d). As discussed previously, the a_{dg}/a_{ph} ratio is not constant in time [*Hu et al.*, 2006; *Jolliff et al.*, 2008] even for open ocean waters, although to the first-order gelbstoff absorption was found to covary with chlorophyll concentration globally [*Morel*, 2009].

[27] Separately, a strong relationship was found between a_{dg} and SST ($r^2 = 0.64$, not shown; it is 0.63 for SeaWiFS a_{dg}). As SST is directly related to solar radiation, the a_{dg} seasonal variations clearly show that a_{dg} at this location is regulated by

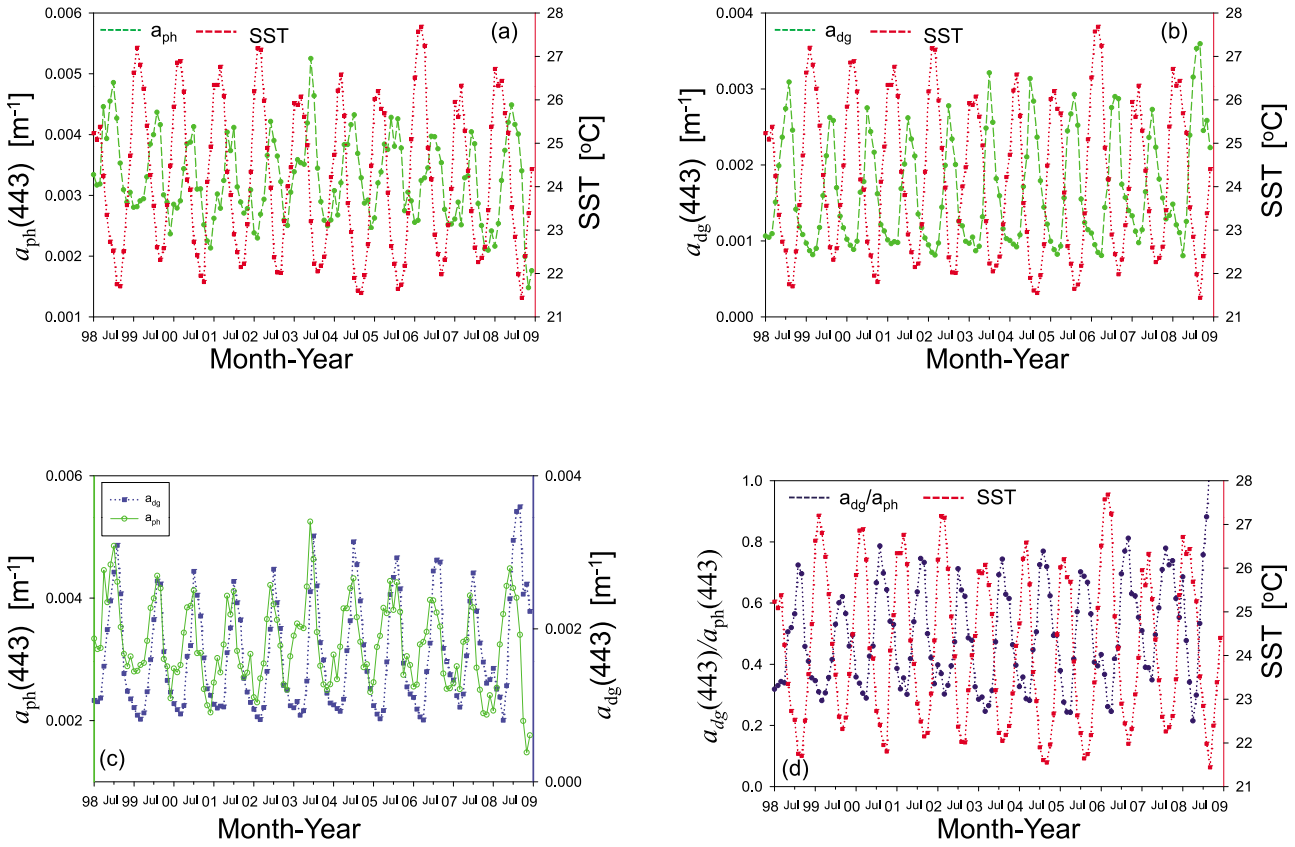

Figure 6. For the 1998–2008 period, monthly time series of (a) a_{ph} and (b) a_{dg}, and their contrast with sea surface temperature (SST; red square symbol with dotted line). (c) The phase difference between a_{ph} and a_{dg}. (d) Seasonal variations of a_{dg}/a_{ph} and its relationship with SST.

phytoplankton degradation as well as solar photobleaching [*Del Vecchio and Blough*, 2002; *Hu et al.*, 2006; *Nelson et al.*, 1998; *Siegel et al.*, 2002; *Twardowski and Donaghay*, 2002].

3.2.3. Interannual Trends From Statistical Analysis and Impacts of Time Frame

[28] Following the approaches in earlier studies [*McClain et al.*, 2004; *Polovina et al.*, 2008], an interannual trend of relevant properties can be drawn with linear statistical analysis. To minimize the effects of seasonal modulation on the evaluation of interannual variations, the interannual trend was analyzed with annual mean of each property. Statistical results from such analyses are presented in Table 1, with "+" indicating an increasing trend and "–" indicating a decreasing trend. It is found that there is a decreasing trend for a_{ph} (r^2 = 0.20) for the 1998–2008 period (r^2 = 0.40 for the 1998–2007 SeaWiFS a_{ph}, also a decreasing trend), but an increasing trend for a_{dg} (r^2 = 0.30) for the same period. The declining trend of a_{ph} is consistent with the evaluations of *Gregg et al.* [2005] for the South Pacific gyre based on empirically derived chlorophyll *a* concentrations (also see Table 1 and section 3.2.4). This apparent declining trend is to a large extent because of the higher a_{ph} (or Chl *a*) values in 1998, which resulted from the strong 1997–1998 El Niño event [*Behrenfeld et al.*, 2001; *Kahru and Mitchell*, 2000; *Susanto and Marra*, 2005]. Excluding the observations of 1998, there is no apparent trend of a_{ph} for the 1999–2008 period (r^2 = 0.04). The increased values of a_{dg} are mainly a result of the higher a_{dg} value in 2008 (resulting from an abnormal drop in MODIS-measured $R_{rs}(412)$, see Figure 7). Omitting the a_{dg} value of 2008, also no apparent trend was found for a_{dg} (r^2 = 0.06).

[29] Clearly, such "trends" are not unequivocal. Either an increase or a decrease over time (trends, and with a different coefficient of determination) could be deduced when different time frames were used for the statistical analysis (see Table 1). Note that such different trends are not sensor dependent as statistical results with products from SeaWiFS alone are nearly the same (see Table 1, except that a_{ph} from SeaWiFS shows no apparent trend for the 1999–2006 period.). These results further demonstrate equivocal interpretations of biogeochemical responses to changes of climate when using such short records. This assertion is further stated given the results of the following analyses, which are focused on the merged time series.

[30] We separated the monthly time series of a bio-optical property into annual background and annual intensity. The annual background is defined as the average low value during Austral summer, while the annual intensity (I) is defined as the difference between the average high value during Austral winter and the average trough during previous summer:

$$I = \text{Peak(in winter)} - \text{Trough(in } \textit{previous} \text{ summer)}. \quad (3)$$

For a_{ph} and Chl *a*, the summer and winter months are December–February and June–August, respectively. Because

Table 1. Trend, Coefficient of Determination (r^2), and Significance Between Time and a_{ph}, a_{dg}, Chl *a*, and SST for Four Separate Time Frames[a]

Property	1998–2003 (P)	1999–2006 (P)	2000–2005 (P)	1998–2008 (P)
$a_{ph}(443)$	−; 0.09 (0.56)	+; 0.15 (0.34)	+; 0.67 (0.05)	−; 0.20 (0.17)
	−; 0.27 (0.29)	−; 0.00 (0.95)	+; 0.35 (0.22)	
$a_{dg}(443)$	−; 0.24 (0.32)	+; 0.65 (0.02)	+; 0.49 (0.12)	+; 0.30 (0.08)
	−; 0.02 (0.80)	+; 0.34 (0.13)	+; 0.63 (0.06)	
Chl *a*[b]	−; 0.22 (0.35)	+; 0.17 (0.31)	+; 0.67 (0.05)	−; 0.05 (0.52)
	−; 0.13 (0.49)	+; 0.04 (0.64)	+; 0.55 (0.09)	
SST	+; 0.04 (0.69)	−: 0.17 (0.31)	−; 0.63 (0.06)	+; 0.00 (0.93)

[a]In the table +, increase; −, decrease; SST, sea surface temperature. The second row for each bio-optical property indicates evaluation results with products solely from SeaWiFS.
[b]Chl *a* here used values derived from the empirical algorithms.

a_{dg} has a different temporal phase from that of a_{ph}, the summer and winter months are February–April and July–September, respectively.

[31] For the 1998–2008 period, the annual background absorption of a_{ph} is ~0.0026 m^{-1} with an intensity of ~0.0013 m^{-1} (see Figure 8a). The background and intensity of a_{ph} also showed different interannual variations, where a more pronounced trend emerged for the background of a_{ph} (a decrease, with $r^2 = 0.24$), but not for the intensity of a_{ph} (an increase, with $r^2 = 0.11$). On the other hand, no significant interannual trend was found for the background of a_{dg} (see Figure 8b), although the a_{dg} intensity suggested an increasing trend. The interannual variations of the a_{ph} background and a_{ph} intensity suggest that even if there is a decrease of phytoplankton at this location in the 1998–2008 period, the decline has happened during the "quiet" period, not during the period when temperature decreases and vertical mixing occurs. Therefore, the dynamics that are responsible for the seasonal increase in phytoplankton pigments has apparently been maintained over the past decade.

[32] These observations add perplexity to the interpretation regarding declining phytoplankton in oceanic gyres. Earlier studies [*Gregg et al.*, 2005; *Polovina et al.*, 2008] showed an interannual decline in averaged chlorophyll *a* concentrations for surface waters in the South Pacific gyre, and speculated that this reduction was a response to increased water temperature (consequently enhancing stratification and reducing nutrient supply from vertical mixing). However, *McClain et al.* [2004] pointed out that for this subtropical gyre (and other gyres [*Palter et al.*, 2005; *Winn et al.*, 1995]), the depth of the nutricline is significantly deeper than the mix layer depth (~250 versus ~100 m) so the supply of nutrients might be mainly associated with surface lateral advection (also see discussions in the work of *Ayers and Lozier* [2010]). Also, the temperature time series did not show a trend ($r^2 = 0.00$) at this site for the 1998–2008 period (see Table 1). In such a scenario, it is less likely that the reduction of phytoplankton pigments in the surface center of the South Pacific gyre results from enhanced stratification, especially when the reduction seems most apparent in the quiet period of each year.

[33] Again, it is necessary to emphasize that interannual trends derived from statistical analyses are sensitive to the time windows used. For instance, if we focus on the years of 1999–2006 (8 years) or 2000–2005 (6 years), a_{ph} actually revealed an increasing trend (see Table 1), further suggesting limitations to infer long-term expectations of oceanic phytoplankton from short observational records [*Henson et al.*, 2009; *Martinez et al.*, 2009]. Such equivocal conclusions might be caused by apparent interannual oscillations (with a cycle of ~6 years, see Figure 8) in the background and intensity of a_{ph} (also Chl *a*, section 3.2.4), and consequently both decreases and increases could be observed when short, but different, time windows were used. Dedicated studies with long-term (multiple decades), consistent, and well-calibrated observations are required to fully account for the physical forces responsible for the interannual variations. Such research will only then provide the fundamentals to

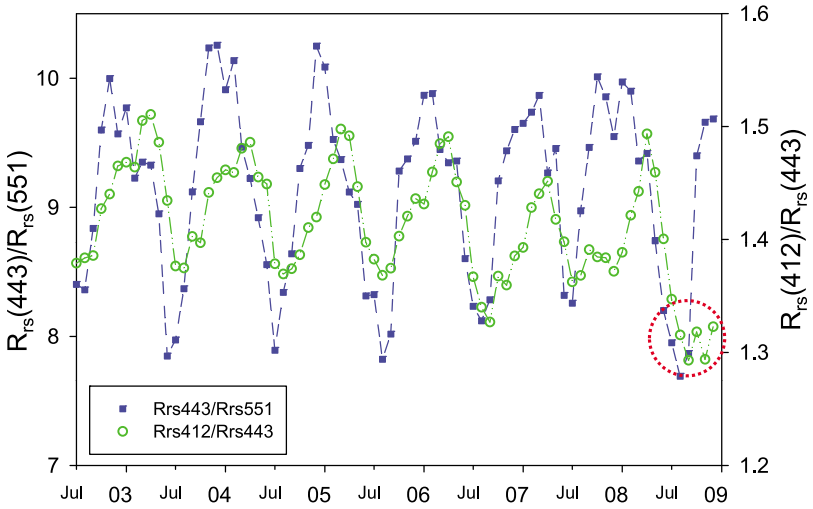

Figure 7. Monthly time series of ratios of $R_{rs}(443)/R_{rs}(551)$ and $R_{rs}(412)/R_{rs}(443)$, where R_{rs} were measured by MODIS. For this study site, an abnormal drop in 2008 Austral winter–spring (circled) is found for the $R_{rs}(412)/R_{rs}(443)$ ratio, which indicates larger a_{dg} for similar a_{ph}. Further study is required to confirm and validate this drop.

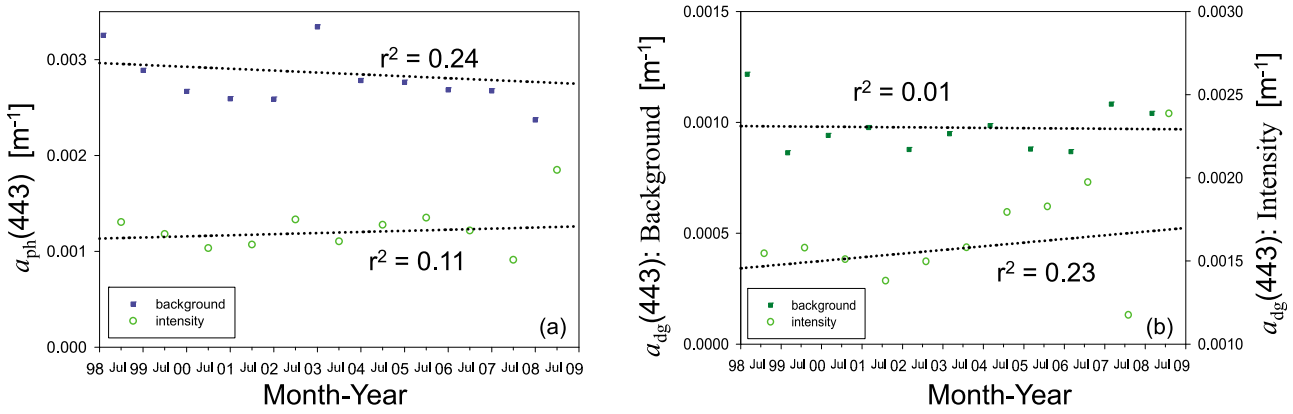

Figure 8. Interannual variations of background and intensity of (a) a_{ph} and (b) a_{dg}.

understand, and then predict, longer-term secular trends [*Henson et al.*, 2009].

3.2.4. Comparison With Empirically Derived Chl *a*

[34] Although time series of phytoplankton absorption can be used to analyze the dynamics of phytoplankton, traditionally such evaluations were based on the time series of empirically derived Chl *a* from satellite-measured ocean color. Figure 9 presents the monthly Chl *a* (derived with standard empirical algorithms) and a_{ph} values (both are merged results of SeaWiFS and MODIS products) for the study site over the 1998–2008 period. Note that a_{ph} could be converted to Chl *a* if the chlorophyll-specific absorption coefficient (a^*_{ph}) is known. We omitted the comparison of Chl *a* here because for the same Chl *a* value a^*_{ph} varies widely, especially for low Chl *a* samples (by a factor of ~3 for low to high values [*Bricaud et al.*, 1995]), and it is not clear yet how to best predict a^*_{ph} value remotely. Instead, the time series of Chl *a* and a_{ph} are compared and contrasted here. In addition, although the empirically derived Chl *a* is on average ~37% lower than sample measured Chl *a* (section 3.1, Figure 4), this difference is assumed to have no impact on analyses of temporal variations or trends as it represents mostly a bias (slope ~1.0 and r^2 ~ 0.94 in linear regression) for this location.

[35] Generally, the two time series show nearly identical seasonal modulations (except October–December 2008 where a higher a_{dg} resulted from low MODIS R_{rs}(412) caused smaller a_{ph}) and interannual variations (also see Table 1). This observation suggests that products from both data-processing approaches are consistent in representing phytoplankton signal (and then interannual trends) at this location. This consistency results from the facts that (1) Chl *a* derived with the OC4v4 (or OC3m) algorithm (R_{rs}(443)/R_{rs}(55x) is the algorithm input for oceanic waters) actually represents the total absorption at 443 nm for such waters (r^2 is 0.97 between QAA-derived *a*(443) and empirically derived Chl *a*, see Figure 10) and (2) the absorption of CDOM and detritus makes relatively small contributions to the total absorption at 443 nm (Figure 6d).

[36] However, there are differences between the two time series. First, the empirically derived Chl *a* shows a stronger seasonal Chl *a* intensity (see Figure 11, a near doubling of Chl *a* during the winter bloom [*McClain et al.*, 2004]). The apparent stronger seasonal bloom is partially due to the systematic bias of the empirically derived Chl *a* (underestimation by 0.01 mg/m^3, see Figure 4) and, consequently, the summer Chl *a* from R_{rs} could be too low. When a value of 0.01 mg/m^3 is added to the time series, the relative seasonal intensity is

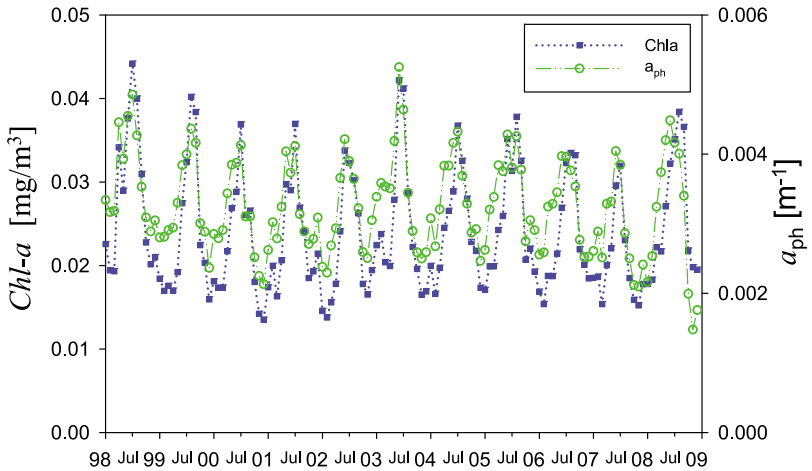

Figure 9. Merged monthly time series of Chl *a* (blue solid squares) and a_{ph} (open circles), with a_{ph} slightly peaking ahead of Chl *a*.

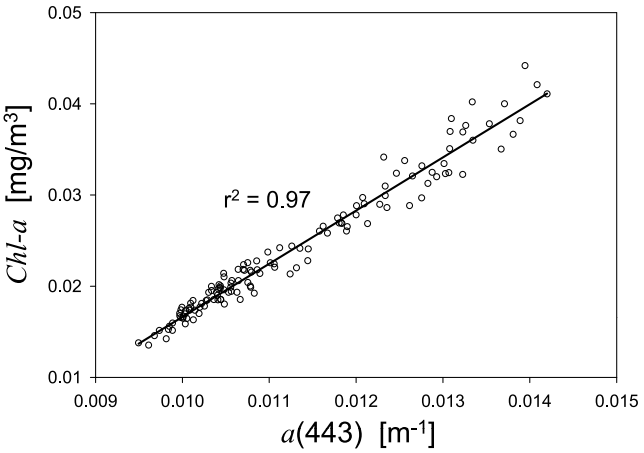

Figure 10. Relationship between Quasi-Analytical-Algorithm-derived $a(443)$ and empirically derived Chl a of the study site, with both properties retrieved from monthly R_{rs} measured by SeaWiFS and MODIS.

reduced. In addition, because of the impact of CDOM and detritus, the strong seasonal elevation of a_{dg} (see Figure 5b) is perceived as "growth" of phytoplankton in the empirical algorithm. After removing the effect of a_{dg}, the a_{ph} time series does not show such a strong winter bloom (Figures 5a and 8). The milder seasonal variation can also be deduced when a_{ph} is converted to Chl a with an $a^*_{ph}(443)$ value of 0.11 mg/m^2, where Chl a is found to increase by just ~70% during winter bloom. This $a^*_{ph}(443)$ value is derived with a_p and Chl a values in Table 1 of *Morel et al.* [2007], with $a_{ph}(443)$ approximated as $a_p(420)$. This $a^*_{ph}(443)$ value is also consistent with the average of $a^*_{ph}(443)$ for Chl a = 0.03 mg/m^3 [*Bricaud et al.*, 1995]. Further, the interannual variations of background and intensity derived from the Chl a time series show weaker decline trends (see Figure 11).

[37] The contrast between the time series of a_{ph} (derived semianalytically) and Chl a (derived empirically) further demonstrates that if an accurate description (and thus better understanding and forecasting) of the dynamics of phytoplankton is required, then it is necessary to separate phytoplankton from gelbstoff and detritus in ocean color remote sensing [*Carder et al.*, 1991] even for such extremely oligotrophic waters.

4. Summary

[38] For a site in the surface center of the South Pacific gyre (the clearest waters in the global ocean) and based on measurements of remote sensing reflectance from both SeaWiFS and MODIS (Aqua), we produced an 11 year monthly time series of absorption coefficients of phytoplankton and detritus/gelbstoff and a time series of chlorophyll a concentration (from standard empirical algorithms). The ocean color inversion process for the optical properties is composed of steps to correct the contributions from Raman scattering and validated with in situ measurements made around the South Pacific gyre. The time series of the optical properties show clear seasonalities and, more importantly, their seasonalities follow their own distinct temporal phases. Such results further demonstrate that different physical and biological processes are responsible for the seasonal and interannual variations in the optical properties of this hyperoligotrophic ocean region.

[39] The 11 year monthly time series suggest a decline in phytoplankton pigments and an increase of detritus/gelbstoff over the 1998–2008 period, although statistically the significances are mild. This phytoplankton pigment trend is consistent with that depicted by empirically derived Chl a, and with reports by *McClain et al.* [2004] and *Gregg et al.* [2005] suggesting that changes are happening not only at the fringe, but also at the surface center of the South Pacific gyre. Previous studies [*Gregg et al.*, 2005; *Polovina et al.*, 2008] speculated that the decrease of chlorophyll in the gyres is a response to reduced nutrient supply due to increased stratification. However, the results here (especially the time series of a_{ph} annual background and a_{ph} annual intensity)

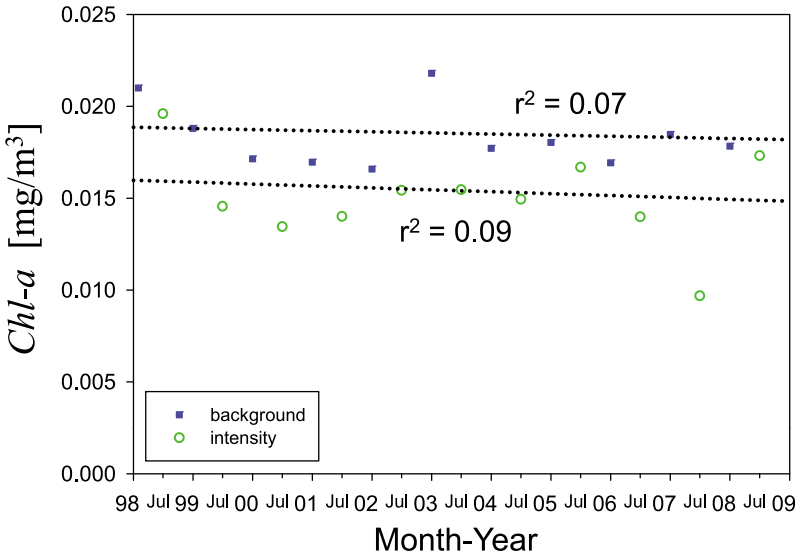

Figure 11. As in Figure 8, interannual variations in the background and intensity of Chl a (derived from the empirical algorithms, see text).

demonstrate a more complex picture. This is because (1) the statistical results (or interannual trends) are sensitive to the time windows used for regression analysis, (2) nutrient supply is less likely from deepwater [*McClain et al.*, 2004], and (3) the observed reduction of phytoplankton pigments mainly happened during the quiet period where significant stratification is already evident. Therefore, in addition to obtaining interannual trends of biogeochemical properties [*Antoine et al.*, 2005; *Gregg et al.*, 2005; *Polovina et al.*, 2008], it is equally or more important to identify the physical forces and quantify their relative contributions for the seasonal and interannual variations [*Ayers and Lozier*, 2010; *Martinez et al.*, 2009; *Palter et al.*, 2005; *Siegel et al.*, 2008].

[40] Because of the relatively isolated location, changes in biogeochemical properties at the surface center of the gyres could provide important information about the status of the oceans and climate. Consequently, long-term, consistent, and reliable measurements of such properties at this location are an important part of the monitoring of global oceans. For this objective, semianalytical algorithms that separate the contributions of gelbstoff and phytoplankton to the observed ocean color are clearly more appropriate than simple empirical algorithms (which mainly represent changes of the total absorption coefficient), especially for delineating the status and dynamics of the resident phytoplankton community.

[41] **Acknowledgments.** The authors are grateful for the financial support provided by NASA's Ocean Biology and Biogeochemistry Program (Lee, Hu, Lewis), the Naval Research Laboratory (Lee, Arnone), the U.S. Office of Naval Research (Lewis), the Canadian Natural Sciences and Engineering Research Council (Lewis), the National High-Tech Research and Development Programme of China (2006AA09A302, 2008AA09Z108), and the NSF-China (40821063; Shang). We would like to thank Yannick Huot for discussions related to ocean color inversion and Charles McClain for encouraging comments on an earlier version of the manuscript. Comments and suggestions from two anonymous reviewers greatly improved this manuscript.

References

Antoine, D., A. Morel, H. R. Gordon, V. F. Banzon, and R. H. Evans (2005), Bridging ocean color observations of the 1980s and 2000s in search of long-term trends, *J. Geophys. Res.*, *110*, C06009, doi:10.1029/2004JC002620.

Antoine, D., F. d'Ortenzio, S. B. Hooker, G. Bécu, B. Gentili, D. Tailliez, and A. J. Scott (2008), Assessment of uncertainty in the ocean reflectance determined by three satellite ocean color sensors (MERIS, SeaWiFS and MODIS-A) at an offshore site in the Mediterranean Sea (BOUSSOLE project), *J. Geophys. Res.*, *113*, C07013, doi:10.1029/2007JC004472.

Ayers, J. M., and M. S. Lozier (2010), Physical controls on the seasonal migration of the North Pacific transition zone chlorophyll front, *J. Geophys. Res.*, *115*, C05001, doi:10.1029/2009JC005596.

Barnett, T. P., D. W. Pierce, and R. Schnur (2001), Detection of anthropogenic climate change in the world's oceans, *Science*, *292* 270–273.

Behrenfeld, M. J., et al. (2001), Biospheric primary production during an ENSO transition, *Science*, *291*, 2594–2597.

Behrenfeld, M. J., E. Boss, D. Siegel, and D. M. Shea (2005), Carbon-based ocean productivity and phytoplankton physiology from space, *Global Biogeochem. Cycles*, *19*, GB1006, doi:10.1029/2004GB002299.

Behrenfeld, M. J., R. T. O'Malley, D. A. Siegel, C. R. McClain, J. L. Sarmiento, G. C. Feldman, A. J. Milligan, P. G. Falkowski, R. M. Letelier, and E. S. Boss (2006), Climate-driven trends in contemporary ocean productivity, *Nature*, *444*, doi:10.1038/nature05317.

Bricaud, A., A. Morel, and L. Prieur (1981), Absorption by dissolved organic matter of the sea (yellow substance) in the UV and visible domains, *Limnol. Oceanogr.*, *26*, 43–53.

Bricaud, A., M. Babin, A. Morel, and H. Claustre (1995), Variability in the chlorophyll-specific absorption coefficients of natural phytoplankton: Analysis and parameterization, *J. Geophys. Res.*, *100*, 13,321–13,332.

Bricaud, A., M. Babin, H. Claustre, J. Ras, and F. Tièche (2010), Light absorption properties and absorption budget of Southeast Pacific waters, *J. Geophys. Res.*, *115*, C08009, doi:10.1029/2009JC005517.

Carder, K. L., R. G. Steward, G. R. Harvey, and P. B. Ortner (1989), Marine humic and fulvic acids: Their effects on remote sensing of ocean chlorophyll, *Limnol. Oceanogr.*, *34*, 68–81.

Carder, K. L., S. K. Hawes, K. A. Baker, R. C. Smith, R. G. Steward, and B. G. Mitchell (1991), Reflectance model for quantifying chlorophyll a in the presence of productivity degradation products, *J. Geophys. Res.*, *96*, 20,599–20,611.

Cullen, J. J., and P. J. Neale (1994), Ultraviolet radiation, ozone depletion, and marine photosynthesis, *Photosynth. Res.*, *39*, 303–320.

Del Vecchio, R., and N. V. Blough (2002), Photobleaching of chromophoric dissolved organic matter in natural waters: Kinetics and modeling, *Mar. Chem.*, *78*, 231–253.

Franz, B. (2009), Ocean color reprocessing, paper presented at Ocean Color Research Team Meeting, NASA, New York, 4–6 May.

Gordon, H. R. (1979), Diffuse reflectance of the ocean: The theory of its augmentation by chl a fluorescence at 685nm, *Appl. Opt.*, *18*, 1161–1166.

Gordon, H. R. (2005), Normalized water-leaving radiance: Revisiting the influence of surface roughness, *Appl. Opt.*, *44*, 241–248.

Gordon, H. R., and M. Wang (1994), Retrieval of water-leaving radiance and aerosol optical thickness over oceans with SeaWiFS: A preliminary algorithm, *Appl. Opt.*, *33*, 443–452.

Gordon, H. R., O. B. Brown, R. H. Evans, J. W. Brown, R. C. Smith, K. S. Baker, and D. K. Clark (1988), A semianalytic radiance model of ocean color, *J. Geophys. Res.*, *93*, 10,909–10,924.

Gordon, H. R., M. R. Lewis, S. D. McLean, M. S. Twardowski, S. A. Freeman, K. J. Voss, and G. C. Boynton (2009), Spectra of particulate backscattering in natural waters, *Opt. Express*, *17*, 16,192–16,208.

Gregg, W. W., N. W. Casey, and C. R. McClain (2005), Recent trends in global ocean chlorophyll, *Geophys. Res. Lett.*, *32*, L03606, doi:10.1029/2004GL021808.

Henson, S. A., J. L. Sarmiento, J. P. Dunne, L. Bopp, I. Lima, S. C. Doney, J. John, and C. Beaulieu (2009), Is global warming already changing ocean productivity?, *Biogeosci. Discuss.*, *6*, 10,311–10,354.

Hu, C., and K. J. Voss (1997), In situ measurements of Raman scattering in clear ocean water, *Appl. Opt.*, *36*(27), 6962–6967.

Hu, C., K. L. Carder, and F. E. Muller-Karger (2001), How precise are SeaWiFS ocean color estimates? Implications of digitization-noise errors, *Remote Sens. Environ.*, *76*, 239–249.

Hu, C., Z. Lee, F. E. Muller-Karger, K. L. Carder, and J. J. Walsh (2006), Ocean color reveals phase shift between marine plants and yellow substance, *IEEE Geosci. Remote Sens. Lett.*, *3*(2), 262–266.

Huot, Y., A. Morel, M. S. Twardowski, D. Stramski, and R. A. Reynolds (2008), Particle optical backscattering along a chlorophyll gradient in the upper layer of the eastern South Pacific Ocean, *Biogeosciences*, *5*, 495–507.

International Ocean-Colour Coordinating Group (IOCCG) (2006), Remote sensing of inherent optical properties: Fundamentals, tests of algorithms, and applications, in *Reports of the International Ocean-Colour Coordinating Group*, no. 5, edited by Z.-P. Lee, p. 126, IOCCG, Dartmouth, Canada.

International Ocean-Colour Coordinating Group (IOCCG) (2007), Ocean-colour data merging, in *Reports of the International Ocean-Colour Coordinating Group*, no. 6, edited by W. Gregg, p. 68, International Ocean-Colour Coordinating Group, Dartmouth, Canada.

Jolliff, J. K., J. C. Kindle, B. Penta, R. Helber, Z. Lee, I. Shulman, R. Arnone, and C. D. Rowley (2008), On the relationship between satellite-estimated bio-optical and thermal properties in the Gulf of Mexico, *J. Geophys. Res.*, *113*, G01024, doi:10.1029/2006JG000373.

Kahru, M., and B. G. Mitchell (2000), Influence of the 1997–98 EI Niño on the surface chlorophyll in the California Current, *Geophys. Res. Lett.*, *27*(18), 2937–2940.

Lee, Z. P., K. L. Carder, S. K. Hawes, R. G. Steward, T. G. Peacock, and C. O. Davis (1994), A model for interpretation of hyperspectral remote sensing reflectance, *Appl. Opt.*, *33*, 5721–5732.

Lee, Z. P., K. L. Carder, and R. Arnone (2002), Deriving inherent optical properties from water color: A multi-band quasi-analytical algorithm for optically deep waters, *Appl. Opt.*, *41*, 5755–5772.

Lee, Z. P., K. L. Carder, and K. P. Du (2004), Effects of molecular and particle scatterings on model parameters for remote-sensing reflectance, *Appl. Opt.*, *43*, 4957–4964.

Lee, Z. P., A. Weidemann, J. Kindle, R. Arnone, K. L. Carder, and C. Davis (2007), Euphotic zone depth: Its derivation and implication to ocean-color remote sensing, *J. Geophys. Res.*, *112*, C03009, doi:10.1029/2006JC003802.

Lee, Z. P., B. Lubac, D. Gray, A. Weidemann, K. Voss, and M. Chami (2009), Rrs modeling and the BRDF correction, paper presented at Ocean Color Research Team Meeting, NASA, New York, 4–6 May.

Lee, Z. P., R. Arnone, C. Hu, P. J. Werdell, and B. Lubac (2010), Uncertainties of optical parameters and their propagations in an analytical ocean color inversion algorithm, *Appl. Opt.*, *49*(3), 369–381.

Loisel, H., and D. Stramski (2000), Estimation of the inherent optical properties of natural waters from the irradiance attenuation coefficient and reflectance in the presence of Raman scattering, *Appl. Opt.*, *39*, 3001–3011.

Maritorena, S., and D. A. Siegel (2005), Consistent merging of satellite ocean color data sets using a bio-optical model, *Remote Sens. Environ.*, *94*, 429–440.

Marshall, B. R., and R. C. Smith (1990), Raman scattering and in-water ocean properties, *Appl. Opt.*, *29*, 71–84.

Martinez, E., D. Antoine, F. D'Ortenzio, and B. Gentili (2009), Climate-driven basin-scale decadal oscillations of oceanic phytoplankton, *Science*, *326*, 1253–1256.

McClain, C. R. (2009), A decade of satellite ocean color observations, *Annu. Rev. Mar. Sci.*, *1*, 19–42.

McClain, C. R., S. R. Signorini, and J. R. Christian (2004), Subtropical gyre variability observed by ocean-color satellites, *Deep Sea Res., Part II*, *51*, 281–301.

Mobley, C. D. (1994), *Light and Water: Radiative Transfer in Natural Waters*, 592 pp., Academic, New York.

Mobley, C. D. (1995), *Hydrolight 3.0 Users' Guide*, 70 pp., SRI Int., Menlo Park, Calif.

Mobley, C. D., L. K. Sundman, and E. Boss (2002), Phase function effects on oceanic light fields, *Appl. Opt.*, *41*, 1035–1050.

Morel, A. (2009), Are the empirical relationships describing the bio-optical properties of case 1 waters consistent and internally compatible?, *J. Geophys. Res.*, *114*, C01016, doi:10.1029/2008JC004803.

Morel, A., and B. Gentili (1991), Diffuse reflectance of oceanic waters: Its dependence on sun angle as influenced by the molecular scattering contribution, *Appl. Opt.*, *30*, 4427–4438.

Morel, A., B. Gentili, H. Claustre, A. Babin, A. Bricaud, J. Ras, and F. Tieche (2007), Optical properties of the "clearest" natural waters, *Limnol. Oceanogr.*, *52*(1), 217–229.

Mueller, J. L., G. S. Fargion, and C. R. McClain (2003), *Ocean Optics Protocols For Satellite Ocean Color Sensor Validation*, revision 4, 36 pp., NASA, Goddard Space Flight Center, Greenbelt, Md.

Nelson, N. B., D. A. Siegel, and A. F. Michaels (1998), Seasonal dynamics of colored dissolved material in the Sargasso Sea, *Deep Sea Res., Part I*, *45*(6), 931–957.

O'Reilly, J., S. Maritorena, B. G. Mitchell, D. Siegel, K. L. Carder, S. Garver, M. Kahru, and C. McClain (1998), Ocean color chlorophyll algorithms for SeaWiFS, *J. Geophys. Res.*, *103*, 24,937–24,953.

O'Reilly, J. E., et al. (2000), SeaWiFS postlaunch calibration and validation analyses, part 3, in *SeaWiFS Postlaunch Technical Report Series*, edited by S. B. Hooker and E. R. Firestone, p. 58, NASA Goddard Space Flight Cent., Greenbelt, Md.

Palter, J. B., M. S. Lozier, and R. T. Barber (2005), The effect of advection on the nutrient reservoir in the North Atlantic subtropical gyre, *Nature*, *437*, 687–692, doi:10.1038/nature03969.

Polovina, J. J., E. A. Howell, and M. Abecassis (2008), Ocean's least productive waters are expanding, *Geophys. Res. Lett.*, *35*, L03618, doi:10.1029/2007GL031745.

Pope, R., and E. Fry (1997), Absorption spectrum (380–700 nm) of pure waters: II. Integrating cavity measurements, *Appl. Opt.*, *36*, 8710–8723.

Sathyendranath, S., and T. Platt (1997), Analytic model of ocean color, *Appl. Opt.*, *36*, 2620–2629.

Sathyendranath, S., and T. Platt (1998), Ocean-color model incorporating transspectral processes, *Appl. Opt.*, *37*, 2216–2227.

Siegel, D. A., S. Maritorena, N. B. Nelson, D. A. Hansell, and M. Lorenzi-Kayser (2002), Global distribution and dynamics of colored dissolved and detrital organic materials, *J. Geophys. Res.*, *107*(C12), 3228, doi:10.1029/2001JC000965.

Siegel, D. A., D. B. Court, D. W. Menzies, P. Peterson, S. Maritorena, and N. B. Nelson (2008), Satellite and in situ observations of the bio-optical signatures of two mesoscale eddies in the Sargasso Sea, *Deep Sea Res., Part II*, *55*, 1218–1230.

Stavn, R. H., and A. D. Weidemann (1988), Optical modeling of clear ocean light fields: Raman scattering effects, *Appl. Opt.*, *27*, 4002–4011.

Stramski, D., A. Bricaud, and A. Morel (2001), Modeling the inherent optical properties of the ocean based on the detailed composition of the planktonic community, *Appl. Opt.*, *40*, 2929–2945.

Stramski, D., E. Boss, D. Bogucki, and K. J. Voss (2004), The role of seawater constituents in light backscattering in the ocean, *Prog. Oceanogr.*, *61*(1), 27–55.

Susanto, R. D., and J. Marra (2005), Effect of the 1997/98 El Niño on chlorophyll *a* variability along the southern coasts of Java and Sumatra, *Oceanography*, *18*(4), 124–127.

Tedetti, M., R. Sempere, A. Vasilkov, B. Charriere, D. Nerini, W. L. Miller, K. Kawamura, and P. Raimbault (2007), High penetration of ultraviolet radiation in the south east Pacific waters, *Geophys. Res. Lett.*, *34*, L12610, doi:10.1029/2007GL029823.

Twardowski, M. S., and P. L. Donaghay (2002), Photobleaching of aquatic dissolved materials: Absorption removal, spectral alteration, and their interrelationship, *J. Geophys. Res.*, *107*(C8), 3091, doi:10.1029/1999JC000281.

Twardowski, M. S., E. Boss, J. M. Sullivan, and P. L. Donaghay (2004), Modeling the spectral shape of absorption by chromophoric dissolved organic matter, *Mar. Chem.*, *89*, 69–88.

Twardowski, M. S., H. Claustre, S. A. Freeman, D. Stramski, and Y. Huot (2007), Optical backscattering properties of the "clearest" natural waters, *Biogeosciences*, *4*, 1041–1058.

Werdell, P. J., and S. W. Bailey (2005), An improved bio-optical data set for ocean color algorithm development and satellite data product validation, *Remote Sens. Environ.*, *98*, 122–140.

Winn, C. D., L. Campbell, J. R. Christian, R. M. Letelier, D. V. Hebel, J. E. Dore, L. Fujieki, and D. M. Karl (1995), Seasonal variability in the phytoplankton community of the North Pacific subtropical gyre, *Global Biogeochem. Cycles*, *9*, 605–620.

Yentsch, C. S., and D. A. Phinney (1985), Spectral fluorescence: An ataxonomic tool for studying the structure of phytoplankton populations, *J. Plankton Res.*, *7*, 617–632.

Zaneveld, J. R. V., E. Boss, and P. A. Hwang (2001), The influence of coherent waves on the remotely sensed reflectance, *Opt. Express*, *9*(6), 260–266.

Zhang, X., L. Hu, and M.-X. He (2009), Scattering by pure seawater: Effect of salinity, *Opt. Express*, *17*(7), 5698–5710.

Zhang, X. D., M. Lewis, and B. Johnson (1998), Influence of bubbles on scattering of light in the ocean, *Appl. Opt.*, *37*, 6525–6536.

R. Arnone and B. Lubac, Naval Research Laboratory, John C. Stennis Space Center, MS 39529, USA.

C. Hu, College of Marine Science, University of South Florida, St. Petersburg, FL 33701, USA.

Z. P. Lee, Geosystems Research Institute, Mississippi State University, John C. Stennis Space Center, MS 39529, USA. (zplee@ngi.msstate.edu)

M. Lewis, Department of Oceanography, Dalhousie University, Halifax, NS B3H 4J1, Canada.

Y. Li and S. Shang, State Key Laboratory of Marine Environmental Science, Xiamen University, Xiamen 361005, China.